Figure S1. KM plots of RFS with integrin expression in basal breast cancer

Unfavorable RFS probability	**ITGA2,** ITGA5, ITGA6, ITGA7, ITGAV, ITGB1, ITGB3, ITGB6
Favorable RFS probability	ITGA3, ITGA4, ITGA8, ITGA9, ITGA10, ITGA11, ITGA2B, ITGAM, ITGAX, ITGAL, ITGAE, ITGAD ITGB2, ITGB4, ITGB5, ITGB7, ITGB8

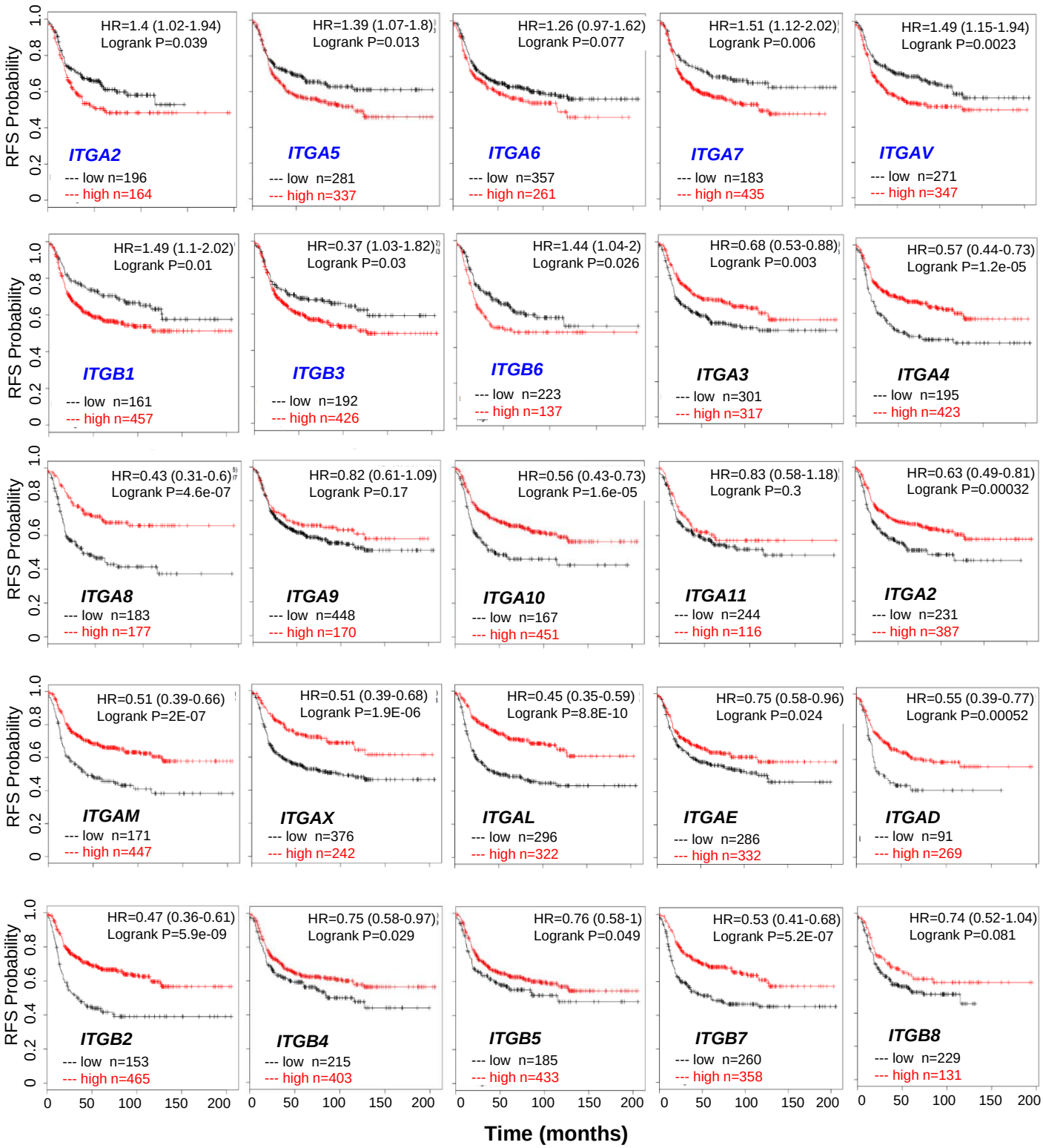

Figure S1. KM plots of RFS with integrin expression in the basal subtype of breast cancers, analyzed using Breast Cancer Kaplan-Meier Plotter**.** Individual KM plots with each subunit gene are based on best cut off and Logrank P<=0.05.

Figure S2. Expression of *ITGA2* in various breast cancer cell lines.

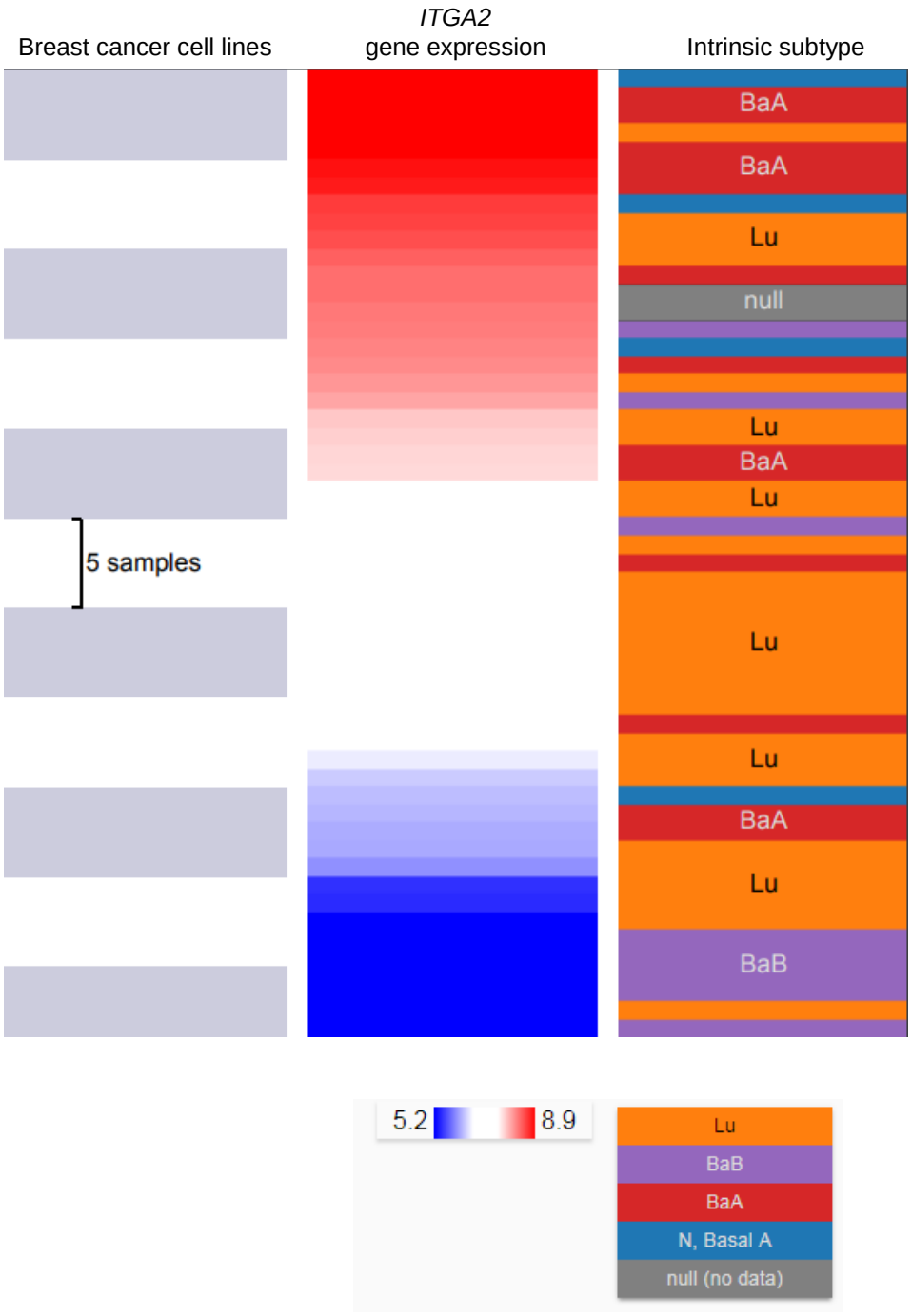

Figure S2. Expression of *ITGA2* in various breast cancer cell lines (related to Fig 1).
UCSF Xena browser-based heatmap of ITGA2 expression across more than 50 cell lines and their corresponding origin of intrinsic subtype of breast cancer.

Figure S3. miR-206 inhibits *ITGA2* expression

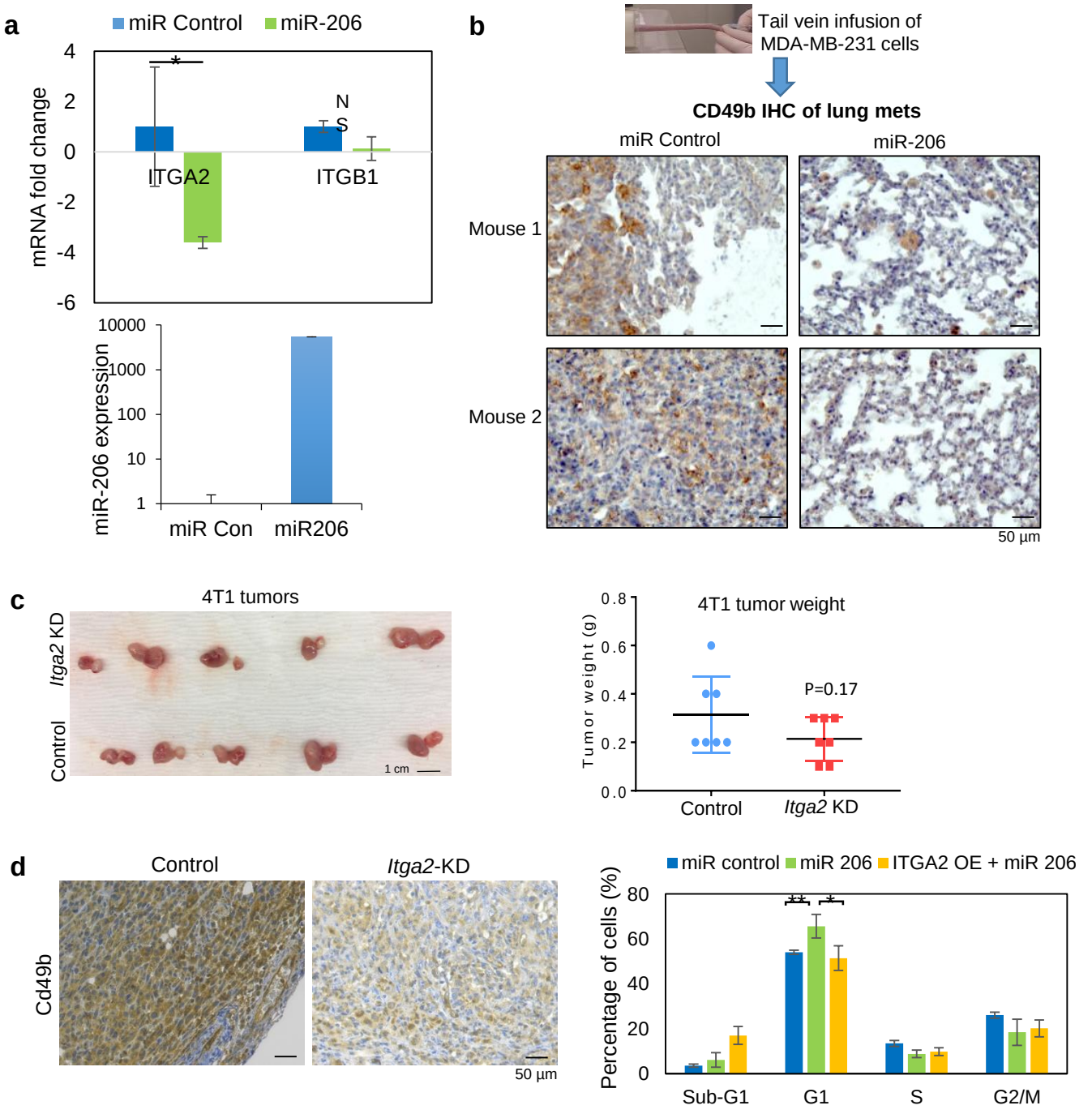

Figure S3. miR-206 inhibits *ITGA2* expression (related to Figs 1-2)

a. Normalized microarray data showing reduced gene expression of ITGA2 (not ITGB1) by transient miR-206 overexpression.

b. Human CD49b IHC staining of lung sections of mice 72 days post tail vein injection of TNBC MDA-MB-231 cells transfected with miR-206 and the miR control, respectively. Scale bars=50 μm.

c. The images (left panel) and weight (right panel) of 4T1 breast tumors mediated by the cells transfected with siRNA control and *siItga2* and orthotopically transplanted into the mammary fat pads of balb/c mice. Scale bar=1 cm. Right panel: *t*-test P=0.17 (n=7, error bars=S.D.)

d. Mouse Cd49b IHC staining of engraft tumors in c at Day 9 post orthotopic implantation of 4T1 cells transfected with KD control and *Itga2 siRNAs*, respectively. Scale bars=50 μm.

Figure S4. *ITGA2* is associated with CD44 and *ITGA2* KD inhibits SOX2 levels and cell confluence.

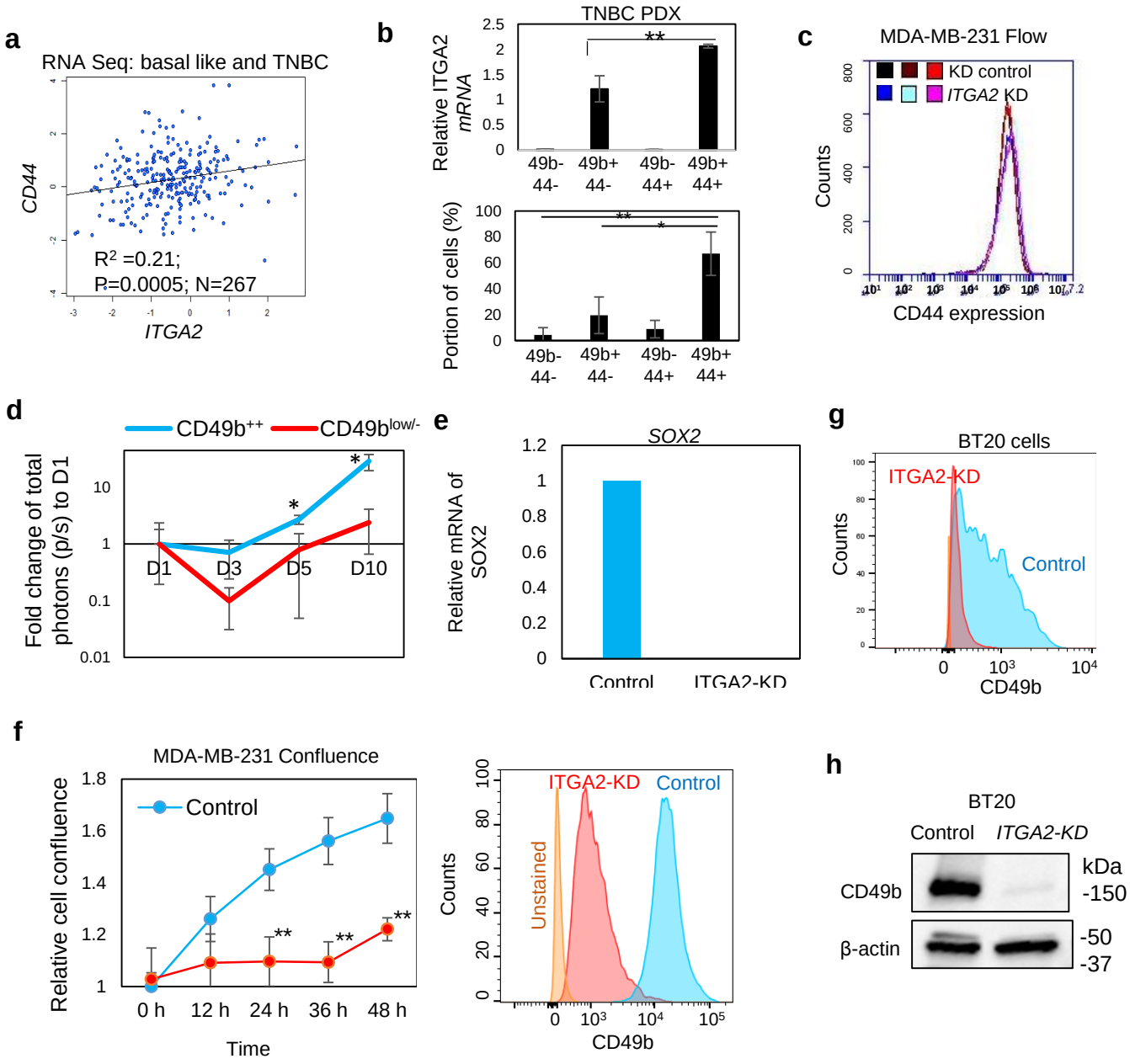

Figure S4. *ITGA2* KD reduces SOX2 expression and cell confluence (related to Fig 3)

a. Gene correlation analyses between *CD44* and *ITGA2* in basal-like and TNBC (n=267) using online Breast Cancer Gene Expression Miner v4.0. Pearson's pairwise correlation coefficient R and P values are shown.

b. Relative *ITGA2* mRNA expression in sorted populations (top panel) and CD49b protein levels (% of populations, bottom panel) in PDX tumor cells, including CD44/CD49b double negative, single positive and double positive cells, measured by RT-PCR (top panel) and flow cytometry (bottom panel), respectively. **P<0.01, *P<0.05 (*t*-test). Error bars=S.D.

c. Flow profiles of CD44 protein expression in MDA-MB-231 cells which were not modulated by *ITGA2* KD.

d. Fold change (Log 10) of $CD49b^{++}$ and $CD49b^{low/-}$ cell-derived tumor burden (total photons, p/s) to Day 1 (D1). *P=0.04 (D5) and 0.02 (D10) (*t*-test). Error bars=S.D.

e. *ITGA2* KD decreased SOX2 mRNA levels in MDA-MB-231 cells, which became undetectable by RT-PCR.

f. Confluence and CD49b expression of MDA-MB-231 cells upon *ITGA2* KD. **t*-test P<0.01 (error bars=S.D.).

g. Flow analyses of reduced CD49b levels in BT20 cells upon *ITGA2* KD.

h. Immunoblot validation for decreased CD49b expression of BT20 cells upon *ITGA2* KD.

Figure S5. Pooled and single si*ITGA2*s caused minimal cell death

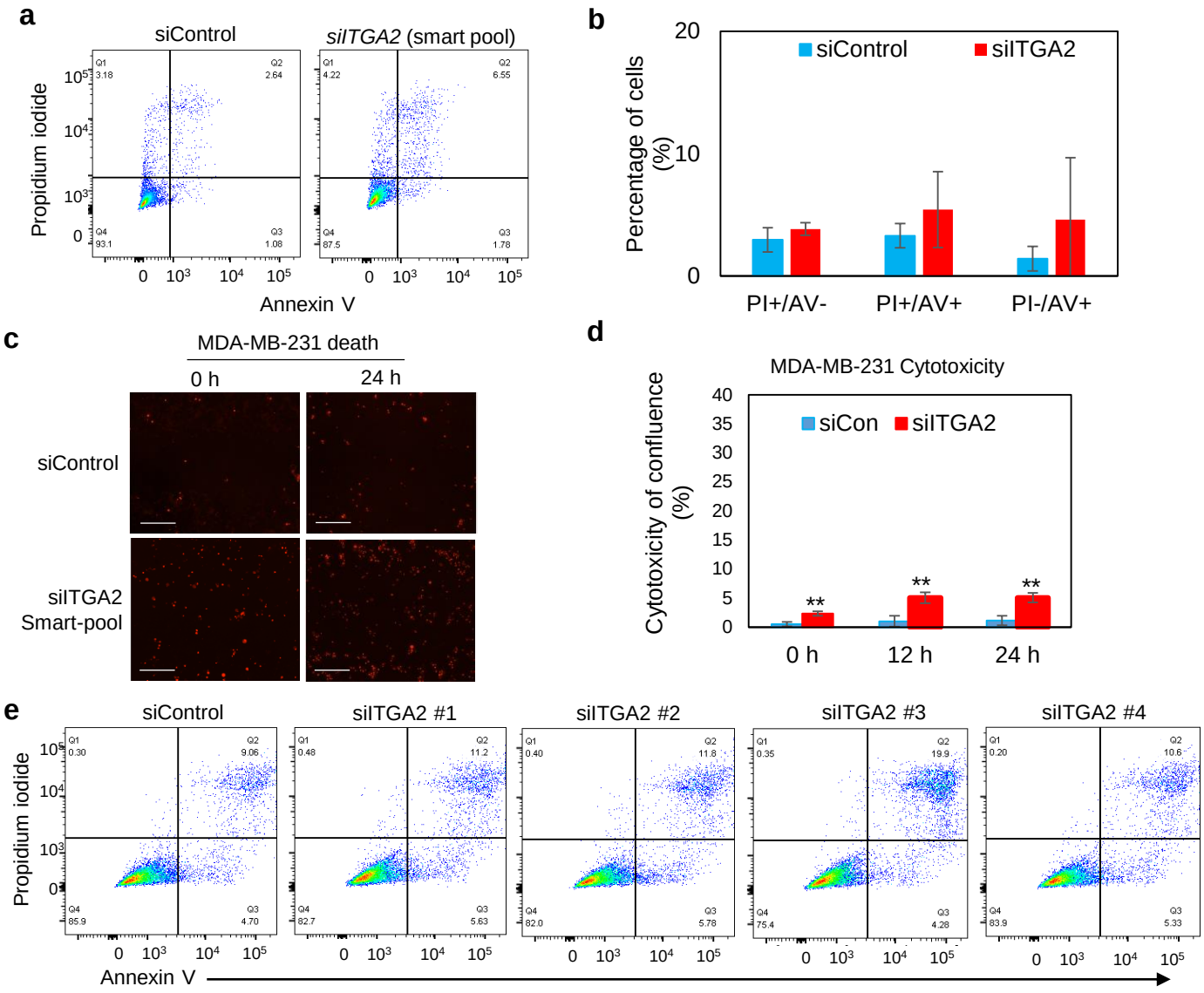

Figure S5. Pooled and single si*ITGA2* caused minimal cell death (related to Fig 3).
a-b. Representative flow dot plots (a) and quantification (b) of cell death measure by Annexin V (AV) /Propidium Iodide (PI), PI^+ and/or AV^+, n=2. **c-d.** si*ITGA2* Smart pool-induced cell death measured by cytotoxic red dye during wound healing (n=3, *t*-test **P<0.01). **e.** Flow plots of AV^+PI^+ MDA-MB-231 cells transfected with individual si*ITGA2* #1-4. (*t*-test **P<0.01, *P<0.05). Error bars=S.D.

Figure S6. Single si*ITGA2*s regulate cell cycle

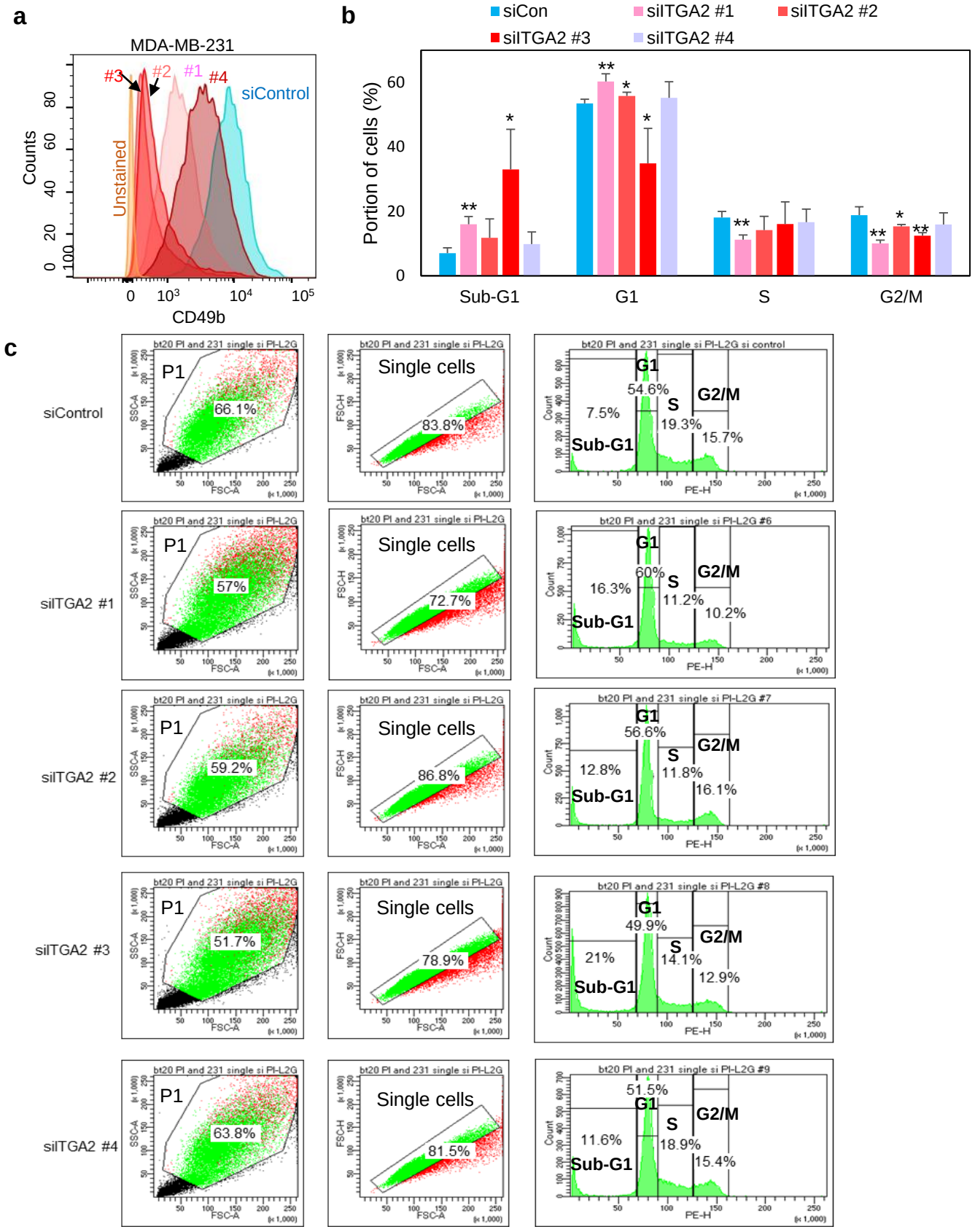

Figure S6. Single si*ITGA2* siRNAs regulate cell cycle (related to Fig 3). a-c. Flow analyses of CD49b (**a**), cell cycle data (**b**), and gated populations from P1 (excluding cell debris), to single cells, and then to subG1, G1, S, and G2/M phases **(c)** in MDA-MB-231 cells transfected with individual si*ITGA2* #1-4 (*t*-test **P<0.01, *P<0.05). Error bars=S.D.

Figure S7. Effects of *ITGA2/Itga2* KD on cell migration and adhesion.

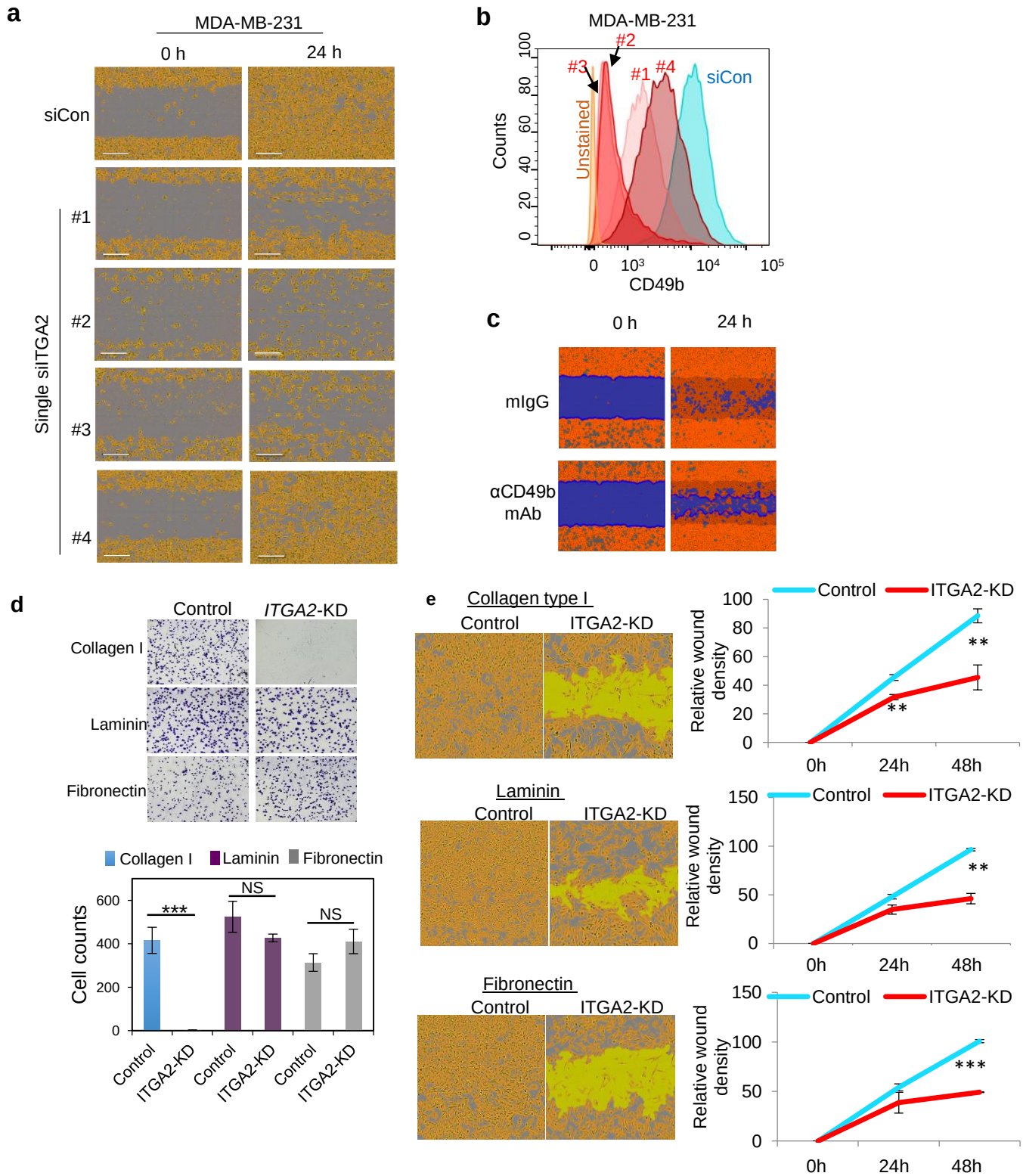

Figure S7. Effects of *ITGA2/Itga2* KD on cell migration and tumor adhesion (related to Fig 4).

a. Migration of MDA-MB-231 cells transfected with individual siITGA2 #1-4 upon the scratched wound healing.
b. Confirmation of reduced CD49b expression upon siITGA2 #1-4 mediated KD
c. Images of slow filling of the scratched wound by MDA-MB-231 cells incubated with anti-CD49b mAb.
d. Images (top panels) and quantified adhesive counts of MDA-MB-231 cells (control and *ITGA2* KD) on collagen I, laminin and fibronectin-coated plates. ***t test P<0.001.
e. Wound-healing migration of MDA-MB-231 cells (control and *ITGA2* KD) on collagen I, laminin and fibronectin-coated plates.

Figure S8. *ITGA2* KD-regulated pathways by RNA sequencing.

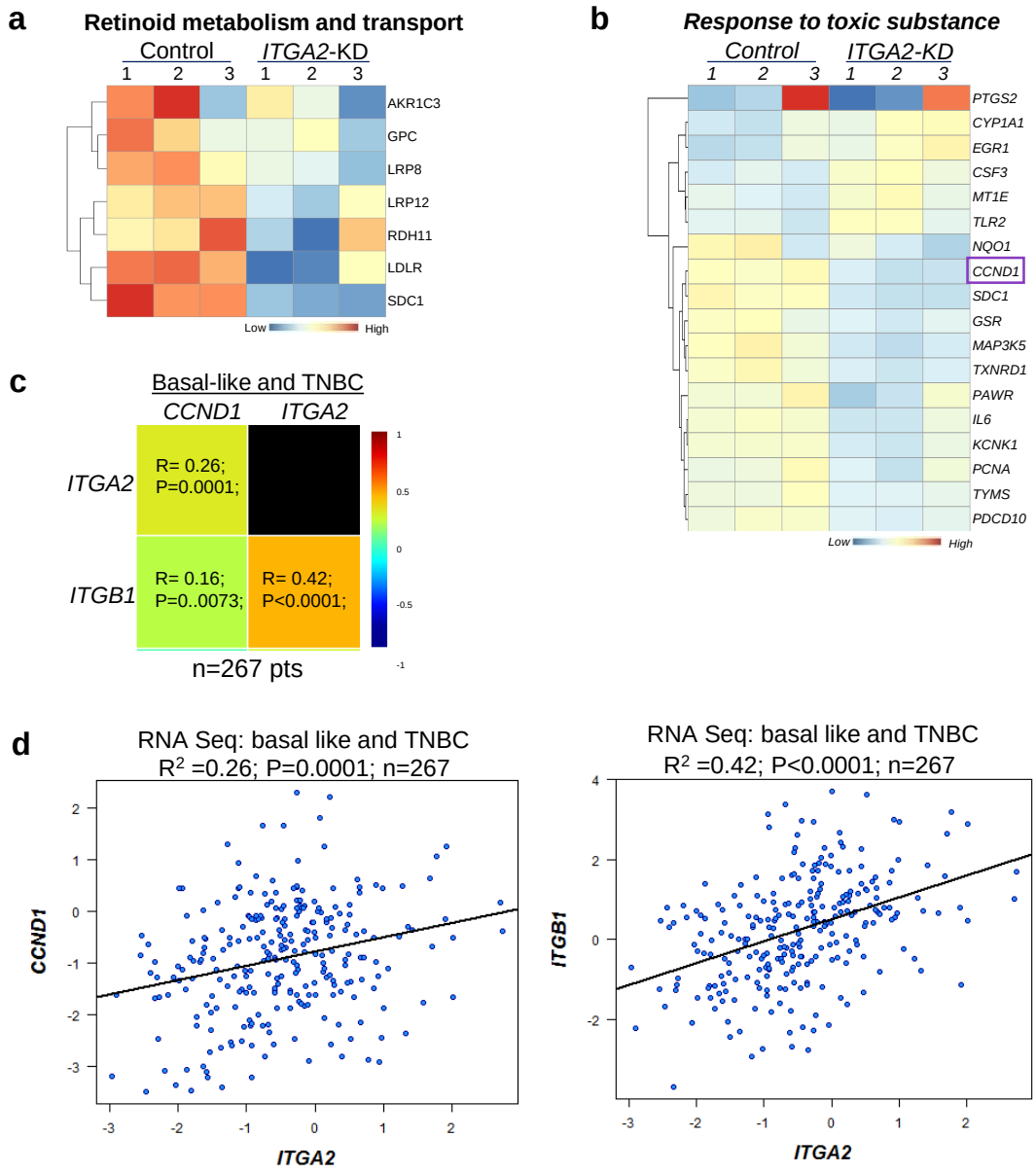

Figure S8. *ITGA2* KD-regulated pathways by RNA sequencing (related to Fig 5).

a-b. Heatmap of genes in representative pathways of retinoid metabolism and transport (**a**), and response to toxic substance (**b**).

c-d. RNA sequencing-based gene correlation map among *ITGA2, CCND1, and ITGB1* (**c**) and correlation plots (**d**) between *CCND1* and *ITGA2* as well as between *ITGB1 and ITGA2* in basal-like and TNBC patients (n=267) using online Breast Cancer Gene Expression Miner v4.0. Pearson's pairwise correlation coefficient R and P values are shown.

Figure S9. ACLY does not contribute to migration phenotype

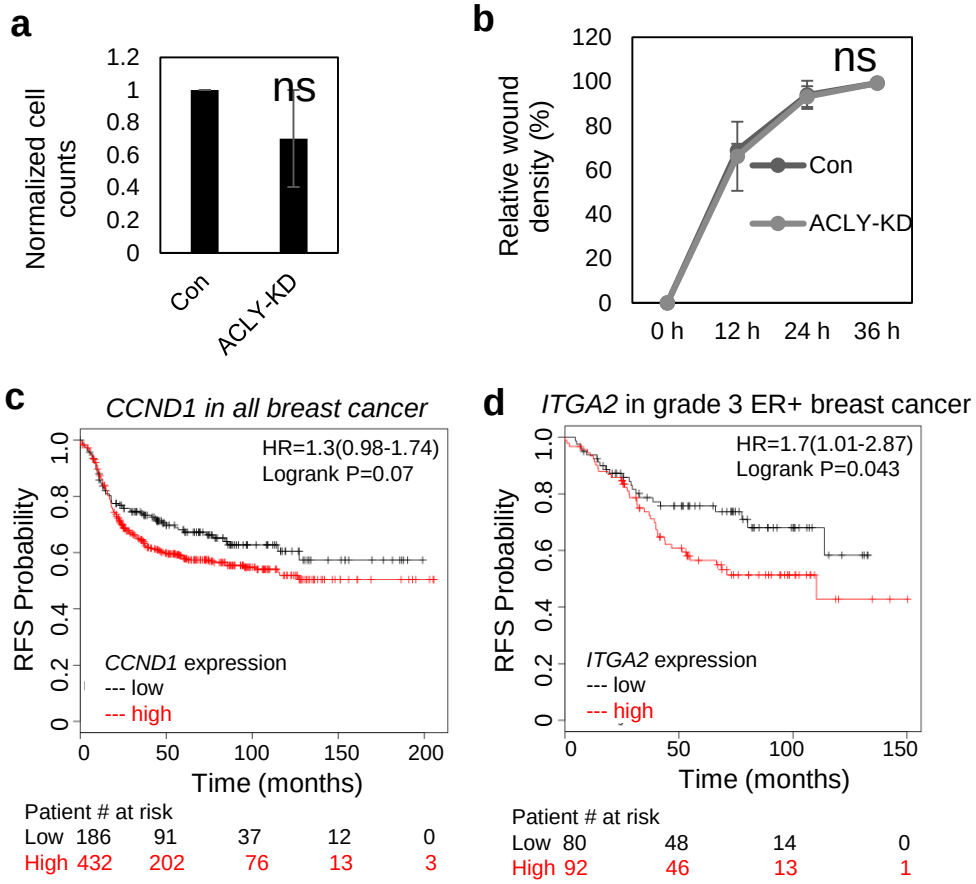

Figure S9. ACLY does not contribute to migration phenotype (related to Figs 6-7).

a. No significant changes of cell counts observed in MDA-MB-231 cells at 48 hour post ACLY knockdown (*ACLY*-KD) compared to the control (Con) (*t*-test P=0.29, N=3 biological replicates). Error bars=S.D.

b. *ACLY* KD did not alter wound healing efficiency of MDA-MB-231 cells, measured by the density of filled cells in the wound (N=3 biological replicates, *t*-test P=0.83, 0.89, and 0.99 for comparisons at 12 h, 24 h, and 36 h respectively). Error bars=S.D.

c. Breast Cancer Kaplan-Meier Plotter analyses of RFS correlated with *CCND1* expression in all breast cancer (Log rank P=0.07, n=618)

d. Breast Cancer Kaplan-Meier Plotter analyses of RFS correlated with *ITGA2* in grade 3 ER+ breast cancer (Log rank P=0.043, n=172).